ROYAL SOCIETY OF CHEMISTRY

PAPER

Check for updates

Synthesis and anti-SARS-CoV-2 potential of novel coumarin hybrids: a combined wet/dry lab approach targeting MPro, Nsp15 and spike protein†

Rukhsana Kausar, Asim Mansha,* Ameer Fawad Zahoor [ID] * and Muhammad Haroon [ID]

This study focuses on the synthesis of novel hybrids with a coumarin scaffold as potential SARS-CoV-2 inhibitors. All the novel coumarin-1,2,4-triazole hybrids **14(a–h)** and phenylacetamide linked coumarin derivatives **17(a–h)** were synthesized by following a standard procedure in good to excellent yields *i.e.*, 51–75% for **14(a–h)** and 62–82% for **17(a–h)**. The synthesized derivatives were subjected to *in silico* modelling to evaluate their anti-SARS-CoV-2 potential, targeting Mpro (main protease), Nsp15 (nonstructural protein) and spike protein. Among all, compounds **14b** and **14c** expressed excellent potency against their respective targets with corresponding binding affinities of −9.5 kcal mol⁻¹ (6VWW), −9.2 kcal mol⁻¹ (6Y84), and −8.6 (6WPT) kcal mol⁻¹, even better than all standards *i.e.*, chloroquine, lopinavir, remdesivir, favipiravir, and nirmatrelvir. The stability of the potent compounds (**14b** and **14c**) was further supported by a 100 ns MD simulation, emphasizing their potent and stable interactions with the main protease, endoribonuclease, and spike protein. The current study highlights the coumarin-based conjugates **14(a–h)** and **17(a–h)** as attractive and promising candidates for future pharmacological interventions against SARS-CoV-2.

1 Introduction

Right from the outset of 2020, a testing situation emerged due to the SARS-CoV-2 (coronavirus) pandemic. This deadly disease affected 774.47 million people around the globe leading to more than 7.03 million deaths.[1] The global healthcare and socio-economic structure have been disrupted significantly due to COVID-19.[2] The healthcare facilities turned out to be over-burdened by the immense responsibility of treating affected people, resulting in a divergence of resources and attention from other important medical needs.[3–9] According to phylogenic research, the main contributory agent of coronavirus is from the sarbecovirus subgenus (genus β-coronavirus).[10,11] It was concluded from different research that the transmission of this deadly pathogenic virus is controlled by ACE2 (host receptor) and RBD (spike protein).[12–20] SARS-CoV-2 had the ability to undergo persistent mutations that spread around the world during COVID-19.[21–25] The new subvariants of COVID (Omicron, delta, beta, and alpha) attenuate the proficiency of known antibody treatment together with antibody-mediated immunity, established *via* infection and vaccination. Therefore, increasing

number of these variants emphasize the need for development of new coronavirus inhibitors.[26] The coronavirus life cycle commences with attachment of spike protein (S protein) with host ACE2 (angiotensin-converting enzyme 2) receptors. The viral genome causes the translation of Nsps (16 non-structural proteins) by confining the host ribosomes and cause the proteolytic cleavage by PLpro and 3Clpro. The sub genome (synthesized from transcription of +ssRNA) translates the structural protein *i.e.*, nucleocapsid (N), membrane protein (M), spike protein (S), and envelop (E). The mature protein and +ssRNA assemble to form new virion after successful transcription and replication of genome. Therefore, main protease, Nsps and spike protein make substantial contribution in transmission and replication. Hence, blocking the activities of these proteins may provide an intriguing therapeutic agent for the treatment of SARS-CoV-2.[27–29] Few traditional and FDA-approved drugs (chloroquine **1**,[30–32] lopinavir **2**,[33–35] remdesivir **3**,[36–38] favipiravir **4**,[39–41] and nirmatrelvir **5** (ref. 42–44)) (Fig. 1) have been known to provide some relief to combat coronavirus, however, there is no particular drug synthesized specifically to combat COVID-19.

The *in silico* modelling analysis brought about a seismic shift in rational drug design by providing a time-effective and economical solution to conventional experimental techniques. By exploiting computational tools, researchers can quickly screen extensive libraries of compounds, detect lead compounds and can enhance their pharmacological features.[45]

Department of Chemistry, Government College University Faisalabad, Faisalabad-38000, Pakistan. E-mail: asimmansha@gcuf.edu.pk; fawad.zahoor@gcuf.edu.pk
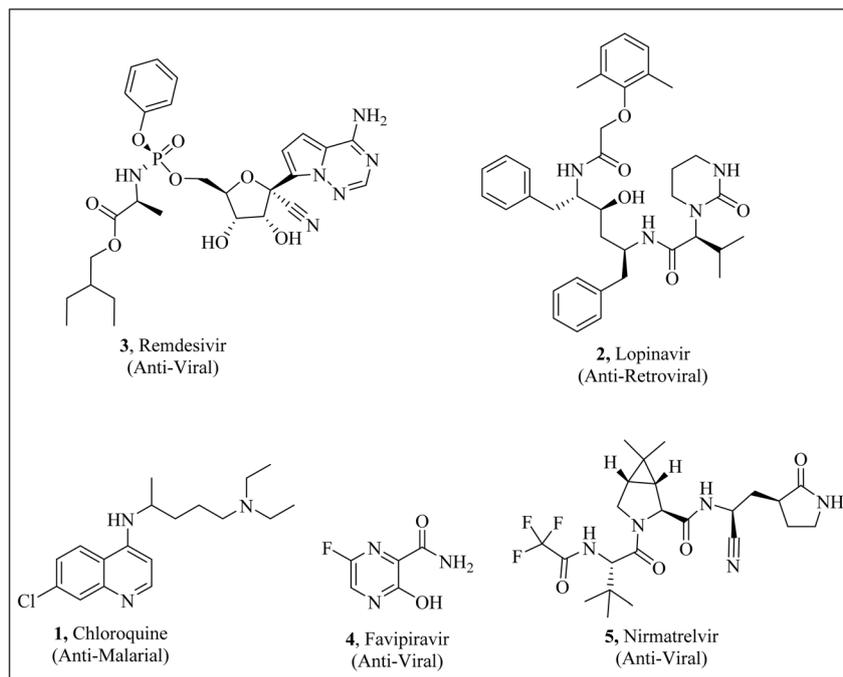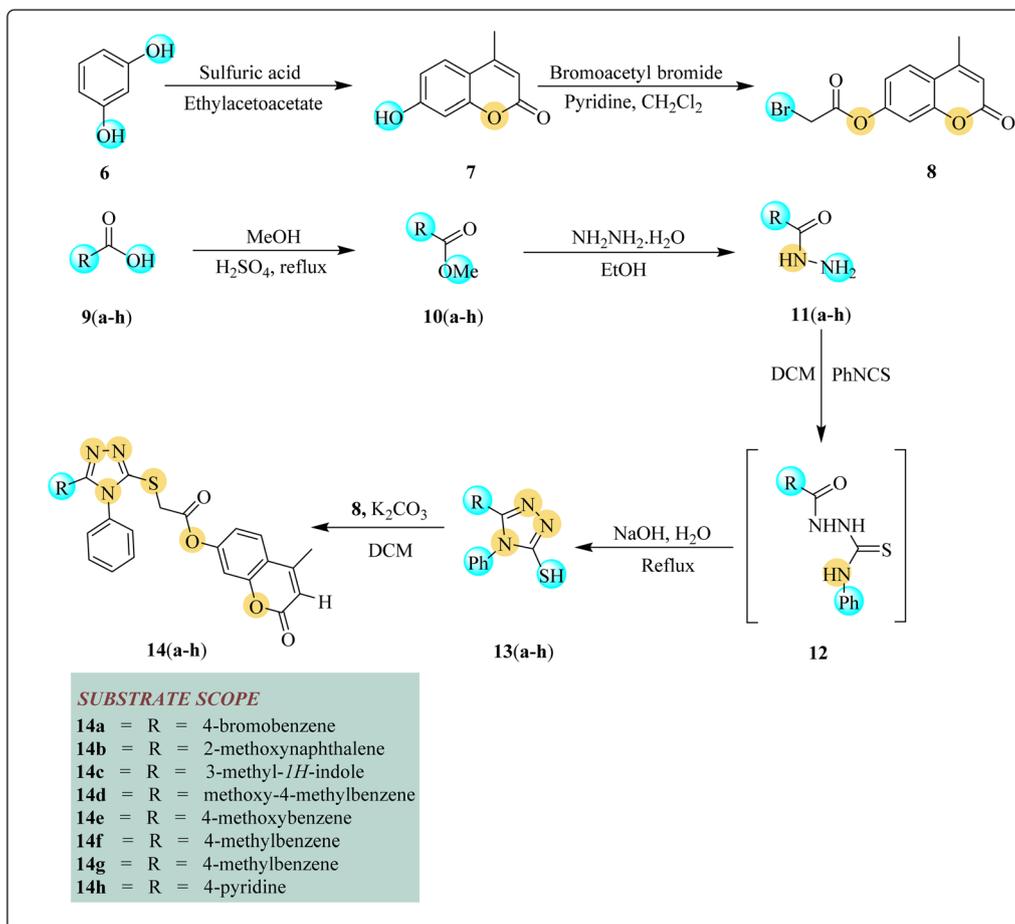
Fig. 1 Structures of important drugs used to combat SARS-CoV-2.

Scheme 1 Synthesis of thio-linked triazole coumarin hybrids 14(a−h).

These strategies facilitate the prediction of toxicity, binding affinities, and pharmacokinetic profiles.[46,47] Additionally, *in silico* modelling approach assists the machine learning algorithms that further enhances the scope of this methodology in drug discovery process.[48]

The heterocyclic compounds[49–51] are important naturally occurring structural motifs[52] found in biologically and pharmaceutically important compounds.[53] Literature survey revealed that these derivatives can act as neuroprotective agents,[54] pesticide agents,[55] anti-Alzheimer agents,[56] anti-fungal agents,[57] anti-oxidative agents,[58] anti-tyrosinase agents,[59,60] anti-mycobacterium tuberculosis agents,[61] and anti-cancer agents.[62] The heterocyclic coumarin scaffolds have also been exploited for designing and synthesizing potential anti-SARS-CoV-2 inhibitors.[63–65] Considering the biological and pharmaceutical potential of coumarin derivatives, we have synthesized novel coumarin hybrids in good to excellent yields. *In silico* computer-aided molecular-docking strategy enables swift-identification of inhibitory potential of targeted molecules. Therefore, all the synthesized coumarin-based conjugates were analyzed using

molecular docking and MD simulation. The complete set of these novel-hybrids were tested against different targets such as 6Y84 (main protease (M^{pro})), 6VWW (Nsp15), and 6WPT (spike protein). These findings may lead to in-future pre-clinical investigations owing to the anti-viral potential of these conjugates against SARS-CoV-2.

2 Result and discussion

2.1. General protocol for construction of thio-linked triazole coumarin hybrids (14a–h)

Initially, resorcinol **6** (1 equivalent) was made to react and stir with ethyl acetoacetate (1 equivalent) in sulfuric acid (few drops) to afford substrate **7** in 73% yield. In the next step, 7-hydroxy-4-methylcoumarin **7** (1 equivalent) and bromoacetylbromide (1 equivalent) were allowed to stir in chloroform (15 mL) and pyridine (1 equivalent) for 16 h to yield bromoacetyl derivative of coumarin **8** (84% yield). By a reaction between methyl alcohol (1 equivalent) and various substituted carboxylic acid **9(a–h)** (1 equivalent), different esters **10(a–h)** were afforded in 72–77%
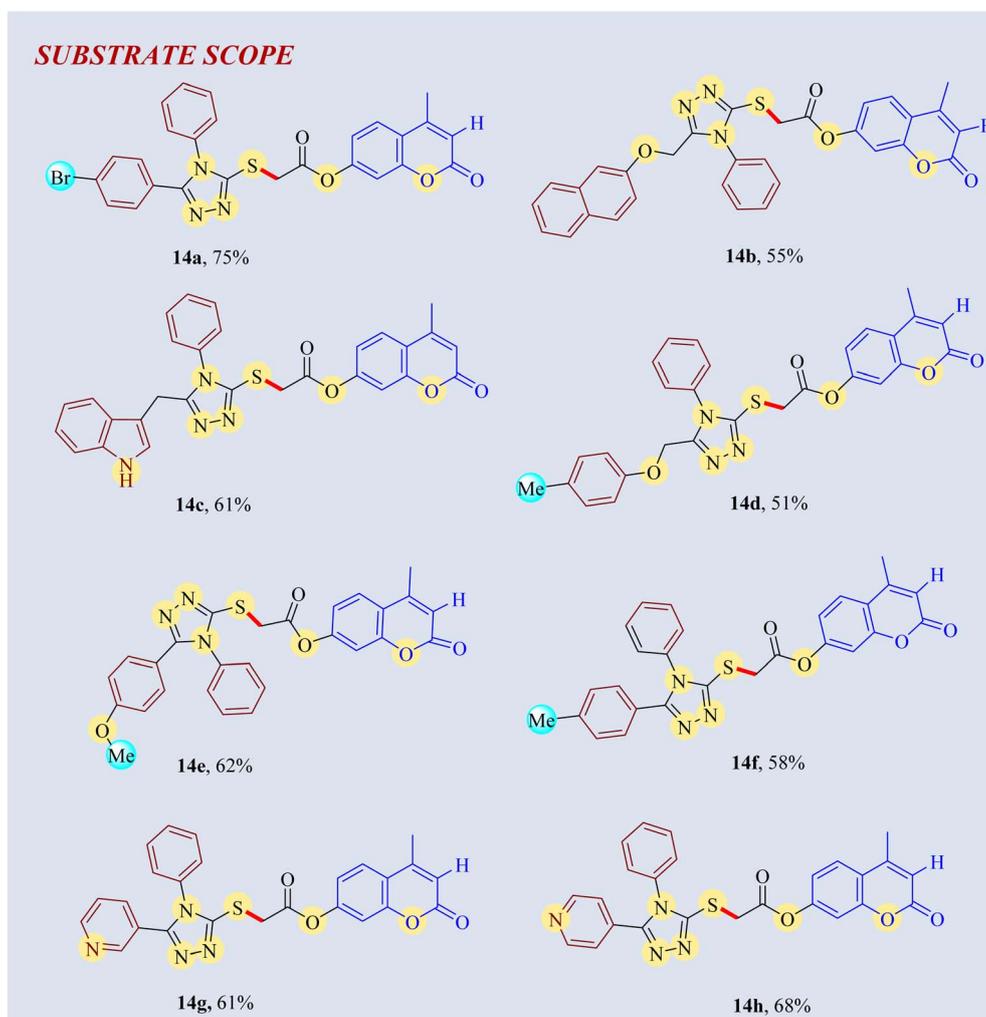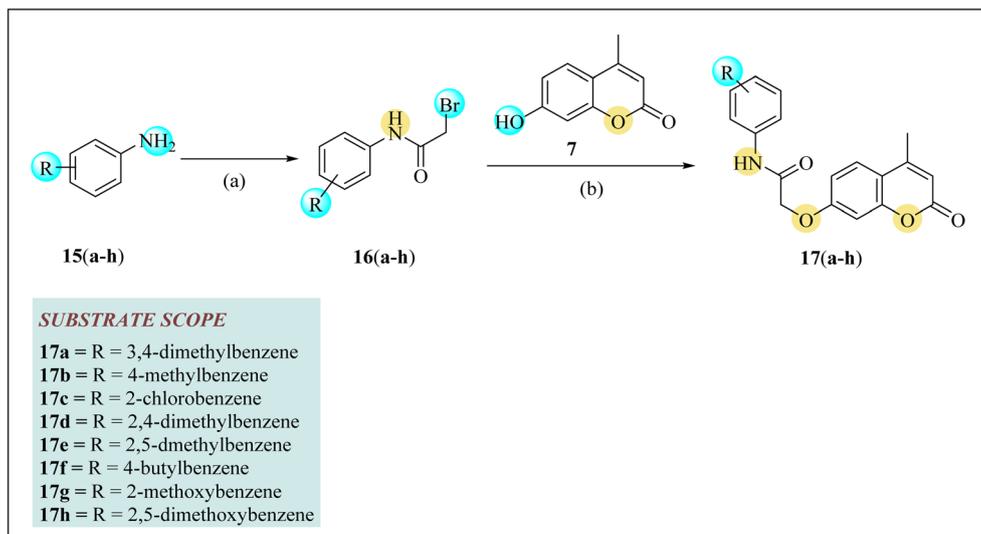

Fig. 2 Substrate scope of coumarin–triazole hybrids **14(a–h)**.

Scheme 2 Reaction protocol of phenylacetamide linked coumarin derivatives **17(a–h)**. Reagents and conditions: (a) 2-bromoacetyl bromide, pyridine, DCM, stirring at 30 °C (b) K_2CO_3, dimethylformamide (DMF).

yields. Esters **10(a–h)** were further converted into hydrazides **11(a–h)** (85–89% yield) by reacting them with hydrazine hydrate in the presence of ethanol. Hydrazides **11(a–h)** were reacted with phenylisothiocyanate in DCM to afford intermediate **12** followed by refluxing it with aqueous sodium hydroxide to yield differently substituted triazoles **13(a–h)** in 75–80% yields.[51] In
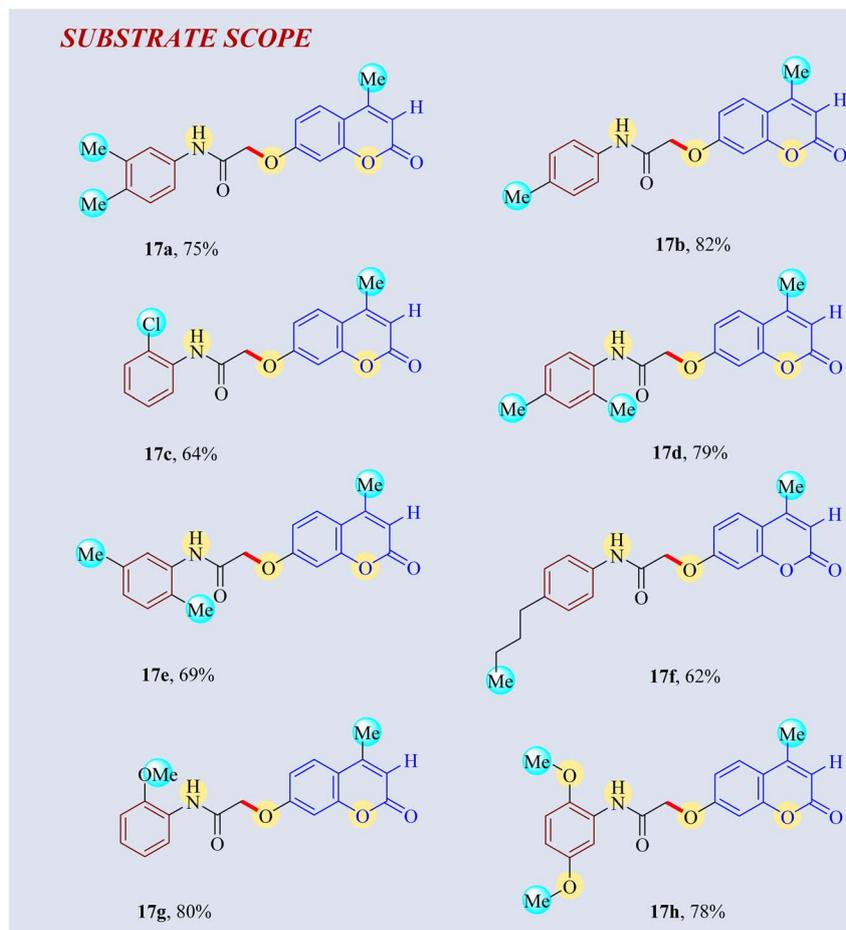

Fig. 3 Substrate scope of phenylacetamide linked coumarin derivatives **17(a–h)**.

the last step, triazoles **13(a–h)** were reacted with bromoacetyl derivative of coumarin **8** in the presence of DCM to afford targeted triazole–coumarin hybrids **14(a–h)**. After the reaction completion, *n*-hexane and water were added to get products' precipitates. These precipitates were recrystallized with ethanol to yield pure targeted coumarin–triazoles hybrids **14(a–h)** in good yields (51–75%) (Scheme 1, Fig. 2).

2.2. Synthesis of phenylacetamide linked coumarin derivatives 17(a–h)

A two-step synthetic approach was applied to afford unreported phenylacetamide linked coumarin derivatives **17(a–h)**. In the first step, a series of variously substituted 2-bromo-*N*-phenylacetamides **16(a–h)** were yielded by the reaction of bromo acetylbromide and different anilines **15(a–h)** in DCM and pyridine. The stirring of 7-hydroxy-4-methyl coumarin **7** with the substituted 2-bromo-*N*-phenylacetamide **16(a–h)** in the presence of K_2CO_3 and DMF (dimethylformamide) yielded the corresponding phenyl acetamide linked coumarin derivatives **17(a–h)** in good yields (62–82%), as outlined in Scheme 2 (Fig. 3).

2.3. Ligand–protein interactions analysis of 6Y84 M^Pro (main protease)

SARS-CoV-2 depends on main protease for effective gene expression and replication.[66] The suppression of main protease (M^Pro) is considered as an efficient route and strategic approach for the treatment of corona virus.[67] The inhibitory potential of all newly synthesized derivatives **14(a–h)** & **17(a–h)** was assessed through molecular docking.[68] The poses with lowest binding scores were selected for interactions study and their binding

affinities were compared with already known inhibitors (chloroquine,[69] lopinavir,[70] remdesivir,[71] favipiravir[72] and nirmatrelvir[73]) potent against SARS-CoV-2. From the results (Table 1), **14c** (-9.2 Kcal mol^{-1}) displayed exceptional binding with M^Pro even better than standards *i.e.*, chloroquine (-5.8 Kcal mol^{-1}), lopinavir -7.1 Kcal mol^{-1}), remdesivir (-7.6 Kcal mol^{-1}), favipiravir (-5.0 Kcal mol^{-1}) and nirmatrelvir (-8.8 Kcal mol^{-1}).

The comprehensive evaluation of compound **14c** with active site of 6Y84 (ref. 74) revealed that the carbonyl group of **14c** interacted with LYS100 (1.73 Å) and TYR101 (2.63 Å) *via* carbon–hydrogen as well as conventional H-bonding interactions, respectively. The aromatic rings of the synthesized hybrid **14c** were revealed to contribute in pi–alkyl and pi–sigma associations with VAL157 and LYS97 having bond distances of 5.22 Å and 2.21 Å, which play a significant role towards the inhibition of SARS-CoV-2.[75–80] (Fig. 4 & 5). In comparison, standards *i.e.*, chloroquine, lopinavir, remdesivir, favipiravir and nirmatrelvir displayed strong hydrogen bonding interactions with ARG298, THR111, THR292, GLN110, ASN151, SER158, ARG4, SER284, TRP207, and ASP289. These standards also established alkyl, π–alkyl, π–π sigma, and pi–pi stacked hydrophobic interactions with PHE294, VAL104, VAL297, VAL303, LYS5, PHE291 and LEU286 (Table 2) (S49, ESI†).

2.4. Ligands–protein interactions analysis of 6VWW endoribonuclease (Nsp15)

The 6VWW endoribonuclease (Nsp15) is accountable for the lysis of viral RNA especially in the case of COVID-19 and assumes a crucial function in eluding innate response of host.[81] The synthesized compounds **14(a–h)** & **17(a–h)** were subjected to molecular docking with 6VWW.[82] As revealed by docking analysis (Table 3), it was found that compound **14b** displayed exceptional binding affinity (-9.5 Kcal mol^{-1}) with the active site of endoribonuclease in comparison with the reference ligands *i.e.*, chloroquine,[69] lopinavir,[70] remdesivir,[71] favipiravir,[72] and nirmatrelvir[73] whose docking scores were observed to be ranging from -6.1 to -9.2 Kcal mol^{-1}.

The ligand–protein interactions disclosed that the ASN200 interacted with the C=O group of **14b** *via* conventional hydrogen bonding at the corresponding distance of 2.75 Å. In addition, coumarin core of **14b** established conventional hydrogen bonding as well as C–H interactions with LYS71 (2.62 Å) and SER198 (3.22 Å), respectively. The naphthyl and coumarin core of **14b** were found to be engaged with VAL295 (4.82 Å), LEU252 (3.63 Å), LYS277 (4.38 Å), LEU266 (5.25 Å), LEU201 (4.47 Å) and PHE259 (5.86 Å) *via* pi–alkyl, alkyl and pi–pi T-shaped hydrophobic interactions (Fig. 6 & 7).[83–85] In comparison, standards *i.e.*, chloroquine, lopinavir, remdesivir, favipiravir, and nirmatrelvir established C–H and conventional hydrogen bonding interactions with LYS71, GLY165, LYS90, ARG199, LYS277, ASP268, SER198, ASN200, SER274, LEU201 and GLN202 (Table 4). Moreover, all of them also interacted with LYS277, LEU252, VAL295, LYS90, TYR279, ARG91, LEU266, SER198, LEU201 and LYS277 *via* hydrophobic interactions (Fig. S50, ESI†).

Table 1 Docking scores of compounds (**14(a–h)** & **17(a–h)**) with binding sites of 6Y84

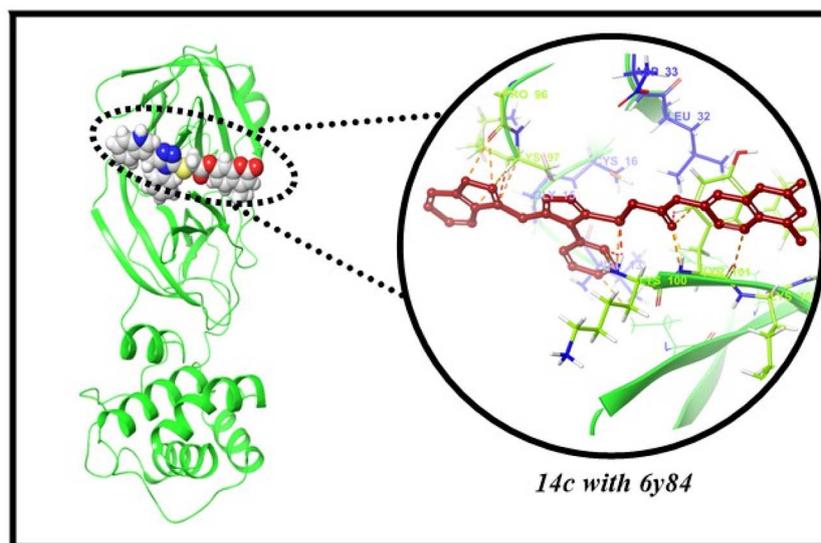| Sr. no.	Compounds	Docking score (Kcal mol^{-1})
1	**14a**	-7.8
2	**14b**	-8.7
3	**14c**	-9.2
4	**14d**	-8.2
5	**14e**	-7.9
6	**14f**	-8.0
7	**14g**	-7.2
8	**14h**	-7.4
9	**17a**	-7.9
10	**17b**	-7.4
11	**17c**	-7.5
12	**17d**	-7.9
13	**17e**	-7.8
14	**17f**	-7.7
15	**17g**	-7.3
16	**17h**	-7.4
17	Chloroquine	-5.8
18	Lopinavir	-7.1
19	Remdesivir	-7.6
20	Favipiravir	-5.0
21	Nirmatrelvir	-8.8

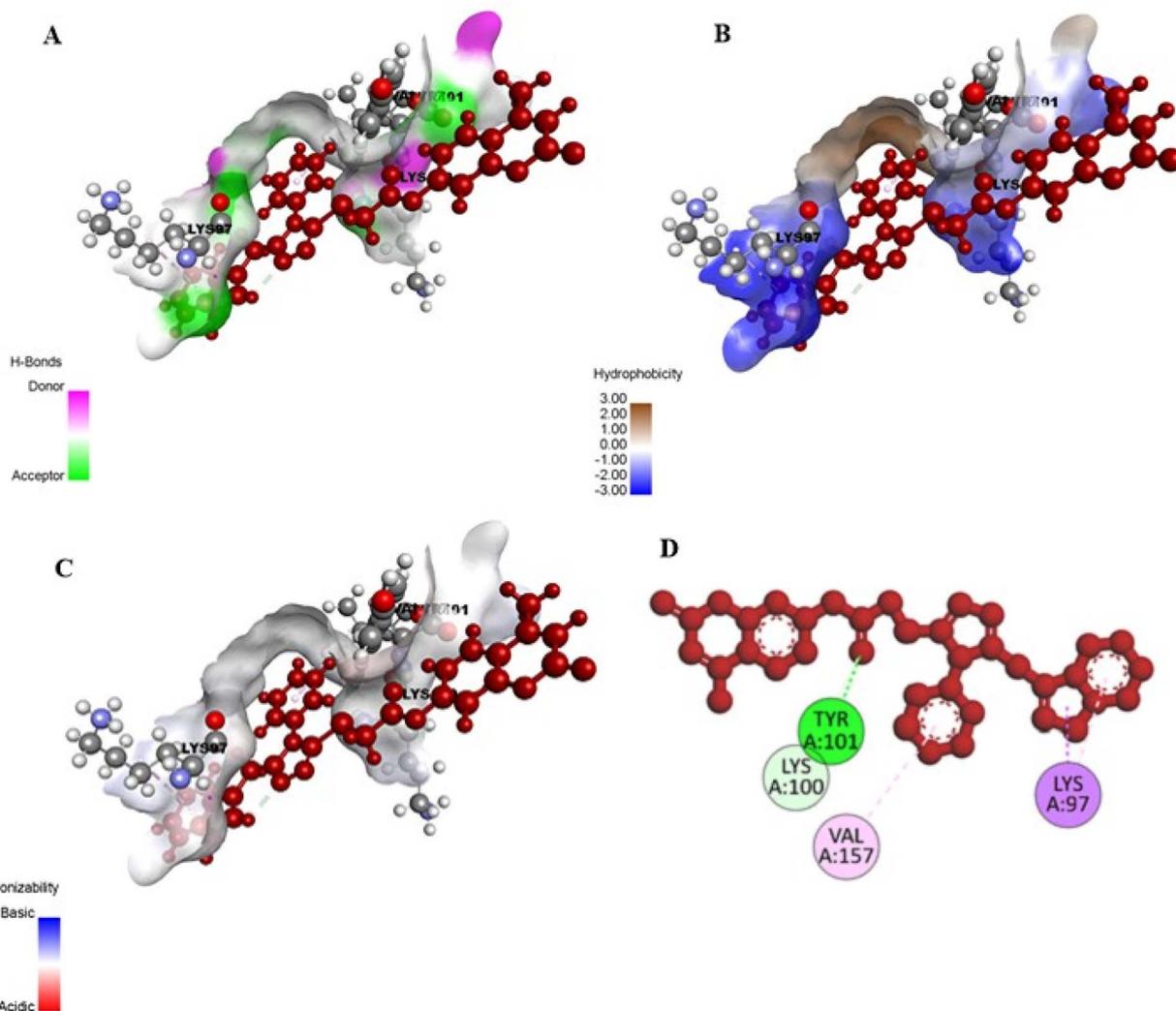**Fig. 4** Interactions of **14c** with binding pocket of 6Y84.

Fig. 5 (A–C) 3D binding interactions of **14c** with 6Y84 receptor. (D) 2D representation of binding analysis of **14c** with 6Y84 receptor.

Table 2 Ligand–protein interactions study of **14(a–h)** & **17(a–h)** with binding sites of 6Y84

Ligand–protein interactions (6Y84)

Sr. no.	Compounds	Hydrophobic interactions			Hydrogen bonding interactions		
		Interacted residues	Interactions	Distance (Å)	Interacted residues	Interactions	Distance (Å)
1	**14c**	VAL157	π–Alkyl	5.22	LYS100	C–H bonding	1.73
		LYS97	π–Sigma, π–alkyl	2.21, 4.24	TYR101	Conventional H-bonding	2.63
2	Chloroquine	PHE294	π–π stacked	4.30	ARG298	Conventional H-bonding	2.83
		VAL104	Alkyl	4.66	THR111	C–H bonding	3.40
					THR292	C–H bonding	3.69
					GLN110	Conventional H-bonding	2.38
3	Lopinavir	PHE294	π–Alkyl	5.21	ARG298	Conventional H-bonding	2.41
		VAL297	π–Alkyl	4.74			
		VAL104	Alkyl	4.59			
		VAL303	π–Sigma	5.11			
4	Remdesivir	PHE294	π–π stacked	3.91	THR111	C–H bonding	2.59
		VAL297	π–Alkyl	4.45	ASN151	Conventional H-bonding	2.73
					SER158	C–H bonding	3.43
5	Favipiravir				ARG298	Conventional H-bonding	2.79
					GLN110	Conventional H–Bonding	2.77
6	Nirmatrelvir	LYS5	Alkyl	4.02	ARG4	C–H bonding	3.46
		PHE291	Alkyl	4.68	SER284	C–H bonding	3.34
		LEU286	Alkyl	4.37	TRP207	Conventional H-bonding	2.28
					ASP289	Conventional H-bonding	1.98

Table 3 Docking scores of compounds (**14(a–h)** & **17(a–h)**) with binding sites of 6VWW

Sr. no.	Compounds	Docking score (Kcal mol^{-1})
1	**14a**	−8.4
2	**14b**	−9.5
3	**14c**	−9.1
4	**14d**	−8.9
5	**14e**	−7.2
6	**14f**	−8.3
7	**14g**	−8.0
8	**14h**	−8.2
9	**17a**	−7.7
10	**17b**	−7.6
11	**17c**	−7.6
12	**17d**	−8.0
13	**17e**	−8.1
14	**17f**	−7.6
15	**17g**	−6.9
16	**17h**	−7.2
17	Chloroquine	−6.1
18	Lopinavir	−7.6
19	Remdesivir	−8.9
20	Favipiravir	−6.1
21	Nirmatrelvir	−9.2

2.5. Ligands–protein interactions analysis of 6WPT (spike protein)

The association of ligand with target receptor 6WPT was also explored using molecular docking. The same docking protocols were used to dock all ligands (**14(a–h)** & **17(a–h)**) with binding pocket of receptor 6WPT. The ligands (**14(a–h)** & **17(a–h)**)

exhibited docking scores between −6.2 to −8.6 Kcal mol^{-1}. Among them, **14c** displayed the highest potency with binding affinity of −8.6 Kcal mol^{-1}. However, chloroquine,[69] lopinavir,[70] remdesivir,[71] favipiravir,[72] and nirmatrelvir[73] interacted with target receptors with binding scores of −5.3, −7.1, −7.0, −6.0, and −8.0 Kcal mol^{-1} respectively (Table 5).

The protein–ligand interaction study revealed that **14c** interacted with coumarin and triazole core by making conventional and C–H bonding interactions with LYS1038 (2.42 Å), SER1037 (3.35 Å), GLY1035 (3.43 Å), and GLN1036 (2.53 Å). The compound **14c** also exhibited strong hydrophobic associations with GLU1031, and TRP886 having bond distances of 4.07 and 4.72 Å (Fig. 8 & 9).[86–88] Additionally, standards *i.e.*, chloroquine, lopinavir, remdesivir, favipiravir, and nirmatrelvir established both hydrophobic interactions (with ALA890, LEU1034, TRP886, LYS1038, LYS90, PRO863, ILE870, PRO862, PHE823 and VAL860) and hydrogen bonding interactions (with TRP886, ARG905, LEU1034, GLY1035, GLN1036, HIS1058, ASP867, THR827, PHE823¸ THR778, ASP867 and THR732) (Fig. S51, ESI†) (Table 6).

2.6. Dynamic simulation studies

Molecular dynamic (MD) simulations present dynamic validation of docking results, facilitating a clearer perception about the structural stability of **14b** and **14c** complexes. Multiple benchmarks such as RMSF, RMSD of C-alpha atoms and protein–ligand interactions have been extracted from the MD trajectories.

2.6.1 RMSD analysis of 14b and 14c with target receptors. MD simulation trajectories are employed to estimate deviation in complexes *via* protein Cα RMSD. The dynamic stability
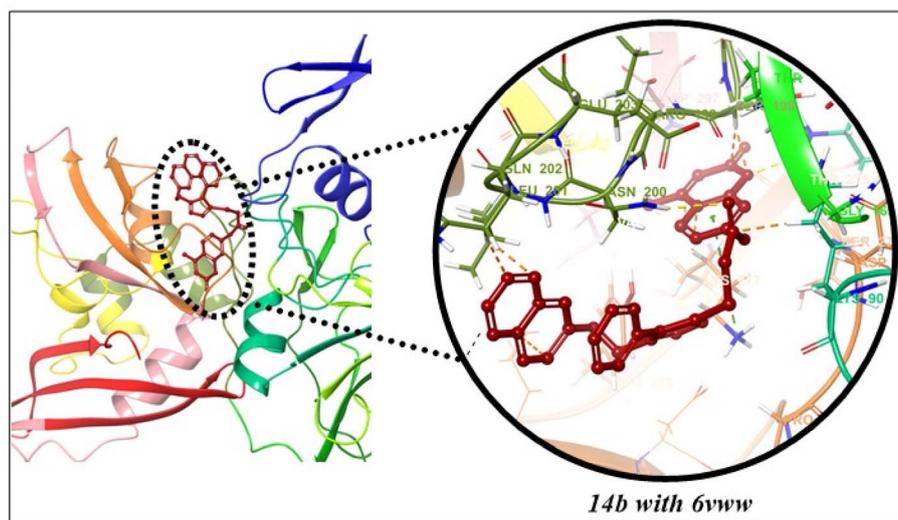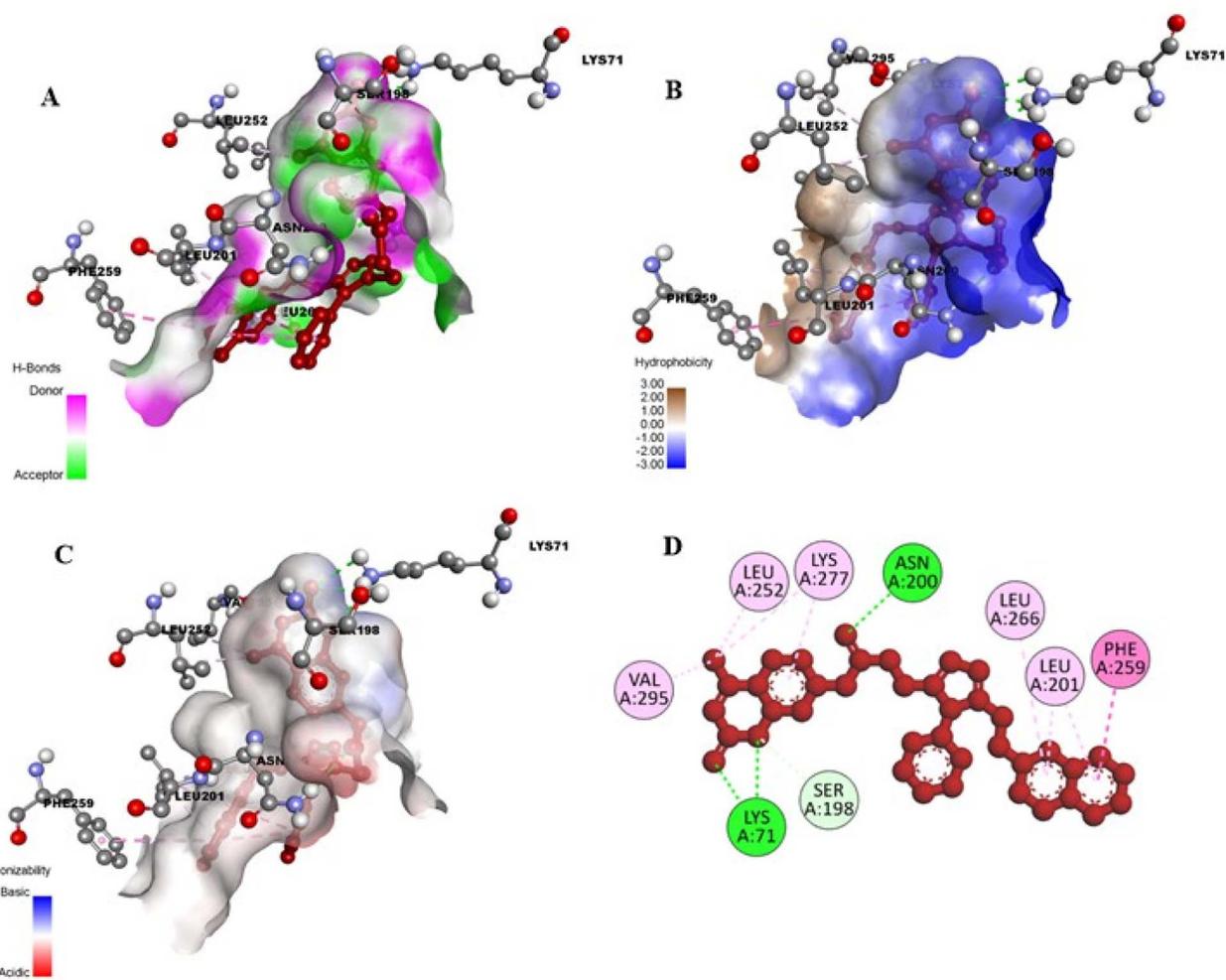
Fig. 6 Interactions of **14b** with 6VWW binding pocket.

Fig. 7 (A–C) 3D binding interactions of **14b** with active site of 6VWW. (D) 2D representation of binding analysis of **14b** with 6VWW receptor.

Table 4 Ligand–protein interactions study of (**14(a–h)** & **17(a–h)**) with binding sites of 6VWW (Nsp15)

Ligand–protein interactions (6VWW)

Sr. no.	Compounds	Hydrophobic interactions			Hydrogen bonding interactions		
		Interacted residues	Interactions	Distance (Å)	Interacted residues	Interactions	Distance (Å)
1	**14b**	VAL295	Alkyl	4.82	ASN200	Conventional H-bonding	2.75
		LEU252	Alkyl	3.63	LYS71	Conventional H-bonding	2.62
		LYS277	Pi–Alkyl	4.38	SER198	C–H bonding	3.22
		LEU266	Pi–Alkyl	5.25			
		LEU201	Pi–Alkyl	4.47			
		PHE259	Pi–Pi T-shaped	5.86			
2	Chloroquine	LYS277	Pi–Alkyl	3.73	LYS71	Conventional H-bonding	2.80
		LEU252	Pi–Alkyl	3.46	GLY165	C–H bonding	3.74
		VAL295	Alkyl	4.53			
		LYS90	Alkyl	4.04			
3	Lopinavir	TYR279	Alkyl	5.04	LYS90	Conventional H-bonding	2.42
		ARG91	Pi–Alkyl	3.68	ARG199	Van der Waals	
		LEU266	Pi–Sigma	3.52 & 4.92	LYS277	C–H bonding	3.10
		SER198	Amide Pi–alkyl	4.53			
		LEU201	Alkyl	3.81			
		LYS90	Pi–Alkyl	5.83			
4	Remdesivir	ARG91	Alkyl	3.36	ASP268	Conventional hydrogen bond	3.22
		LEU266	Alkyl	5.20	LYS90	Conventional hydrogen bond	2.48
		LEU201	Alkyl	4.32	SER198	Conventional hydrogen bond	3.34
		LYS277	π–Alkyl	3.73	ASN200	Conventional hydrogen bond	2.59
5	Favipiravir	LYS90	π–Alkyl	5.01	LYS71	Conventional hydrogen bond	3.54
					SER274	Conventional hydrogen bond	2.30
					ARG199	Conventional hydrogen bond	2.34
6	Nirmatrelvir	LYS90	Alkyl	4.23	LYS90	Conventional hydrogen bond	2.53
					SER274	Conventional hydrogen bond	2.12
					LYS71	Conventional hydrogen bond	2.64
					SER198	C–H bonding	3.39
					LEU201	Conventional hydrogen bond	2.95
					GLN202	Conventional hydrogen bond	2.24

Table 5 Docking scores of compounds (**14(a–h)** & **17(a–h)**) with binding sites of 6WPT

Sr. no.	Compounds	Docking score (Kcal mol^{-1})
1	**14a**	−7.5
2	**14b**	−7.9
3	**14c**	−8.6
4	**14d**	−7.6
5	**14e**	−7.5
6	**14f**	−7.4
7	**14g**	−7.9
8	**14h**	−7.4
9	**17a**	−7.9
10	**17b**	−7.9
11	**17c**	−6.2
12	**17d**	−7.5
13	**17e**	−7.4
14	**17f**	−6.9
15	**17g**	−7.9
16	**17h**	−6.5
17	Chloroquine	−5.3
18	Lopinavir	−7.1
19	Remdesivir	−7.0
20	Favipiravir	−6.0
21	Nirmatrelvir	−8.0

of potent compounds **14b** and **14c** with respective receptors (6VWW, 6Y84 and 6WPT) were assessed through 100 ns MD simulations *via* RMSD. These RMSD calculations of protein–ligand complexes were calculated with reference to the original state, that served as an indicator for determining ligand–protein complex stability. Compound **14b** displayed conformational changes in RMSD during the initial 40 ns, after which moderate stability was attained from 40–100 ns with the 6VWW receptor. Similarly, compound **14c**, when complexed with 6WPT, showed stability in RMSD from 35–100 ns after an initial conformational change period. Additionally, **14c** exhibited slight deviations with the binding pocket during the initial 0–35 ns period, after which higher stability was attained between 35–100 ns with main protease (6Y84) (Fig. 10).

2.6.2 RMSF analysis of potent 14c and 14b complexes. During MD simulation period, average deviation of each protein residue from its initial position is calculated *via* RMSF. Moreover, stability of each complex is determined by RMSF of corresponding amino acid. The analysis of MD simulation *via* RMSF unearthed new observations about the flexibility of protein–ligand complexes with individual residues. During MD simulation period, complexes with relatively higher RMSF values tend to be more flexible as compared to those having
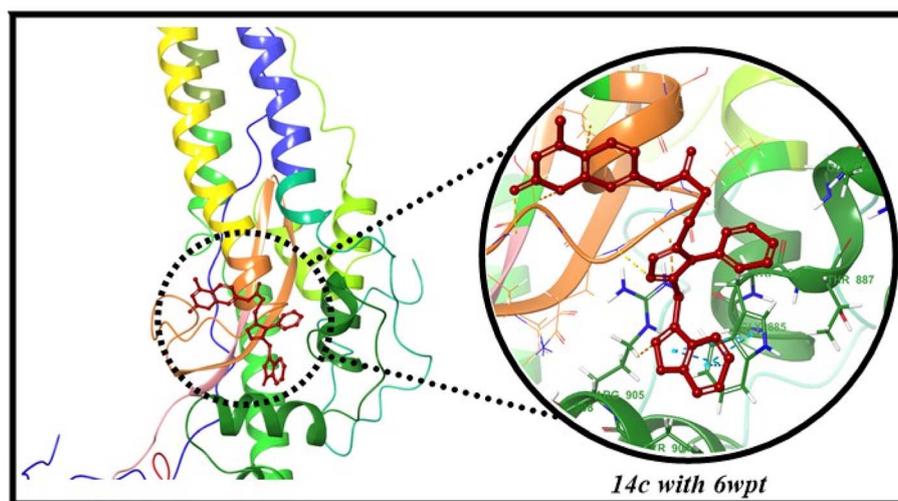
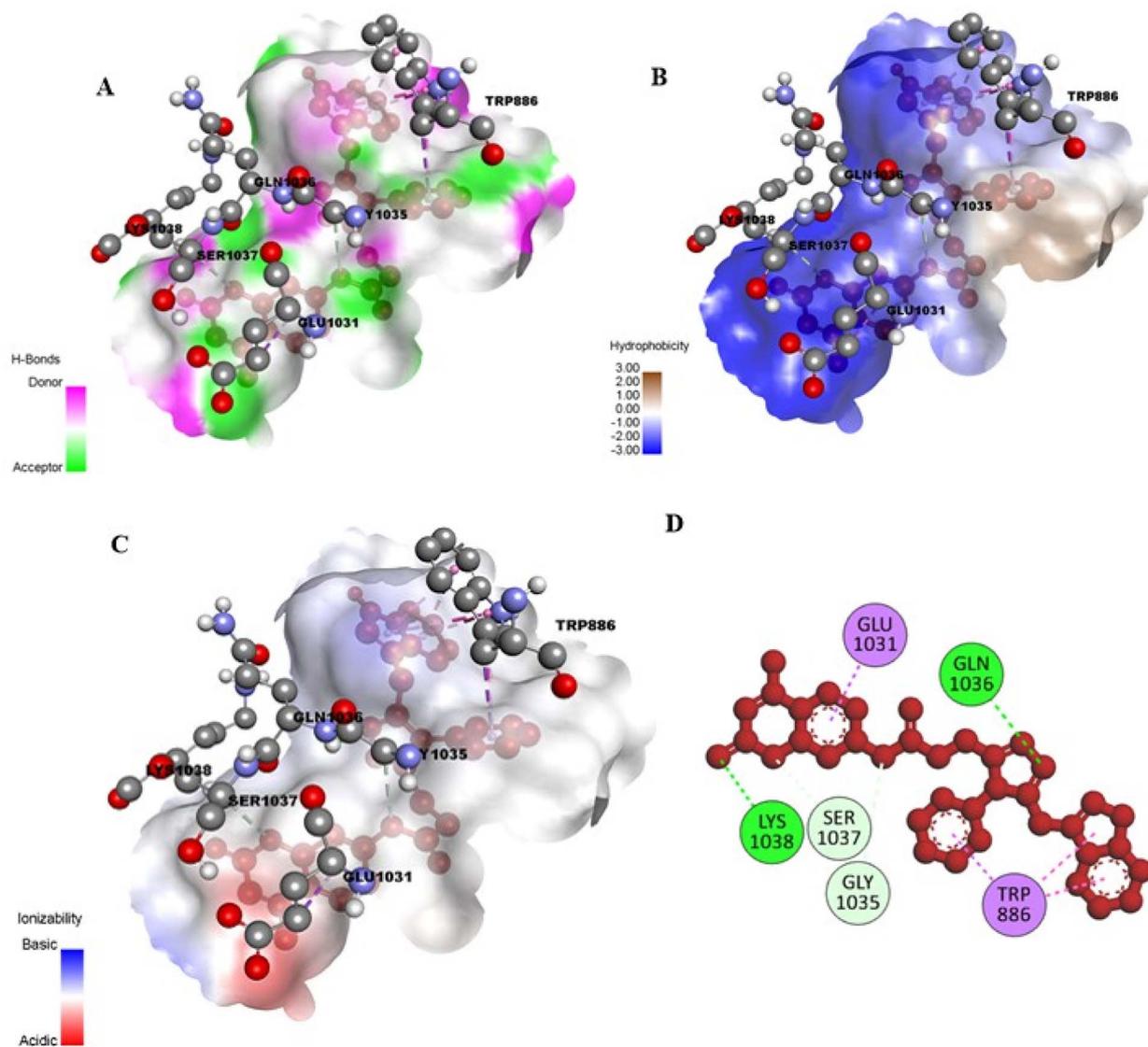Fig. 8 Interactions of **14c** with active site of 6WPT receptor.

Fig. 9 (A–C) 3D interactions of potent compound **14c** with spike protein. (D) 2D representation of binding analysis of **14c** with 6WPT receptor.

Table 6 Ligand–protein interactions study of (**14(a–h)** & **17(a–h)**) with binding sites of 6WPT

		Hydrophobic interactions			Hydrogen bonding interactions		
Sr. no.	Compounds	Interacted residues	Interactions	Distance (Å)	Interacted residues	Interactions	Distance (Å)
1	**14c**	GLU1031	Pi–sigma, Pi–Pi T-shaped	4.07	GLN1036	Conventional H-bonding	2.53
		TRP886	Pi–sigma, Pi–Pi stacked	4.72	LYS1038	Conventional H-bonding	2.42
					GLY1035	C–H bonding	3.43
					SER1037	C–H bonding	3.35
2	Chloroquine	ALA890	Alkyl	4.21	ARG905	C–H bonding	3.41
		LEU1034	Pi-alkyl	4.85	TRP886	C–H bonding	4.48
					LEU1034	Conventional H-bonding	2.72
3	Lopinavir	LEU1034	Alkyl	4.19	GLY1035	C–H bonding	3.35
		ALA890	Alkyl	4.13	GLN1036	Conventional H-bonding	2.06
		TRP886	π–π stacked	3.87			
		LYS1038	Alkyl	4.17			
		LYS90	Pi-alkyl	5.83			
4	Remdesivir	PRO863	Alkyl	4.96	HIS1058	C–H bonding	2.64
		ILE870	Alkyl	4.82	ASP867	Conventional hydrogen bond	3.35
					THR827	Conventional hydrogen bond	2.09
					PHE823	Conventional H-bonding	2.50
5	Favipiravir	PRO863	π–Alkyl	4.64	THR778	Conventional H-bonding	2.59
6	Nirmatrelvir	PRO862	Pi-alkyl	4.95	ASP867	Conventional H-bonding	1.79
		PHE823	Alkyl	5.09	THR732	Conventional H-bonding	2.49
		VAL860	Pi–alkyl	5.30	HIS1058	Conventional H-bonding	1.91
		PRO863	Pi–alkyl	4.74			

low RMSF values. Compound **14b** exhibited minimal fluctuations, ranging from 0.8 to 2.4 Å, at residues 55–250 of 6VWW receptor. Similarly, compound **14c** exhibited a similar fluctuation profile with the spike protein, achieving stability between 0.8–2.9 Å at residues 25–325, after which higher fluctuations were observed between residues 350–400. Additionally, compound **14c** displayed slightly higher fluctuations due to conformational changes between residues 25–75, after which minimal fluctuations were observed within a range of 0.6–2 Å. The corresponding RMSF analysis images have been presented in Fig. 10.

2.6.3 Protein–ligand contacts 14b and 14c with target receptors. To interpret the suppressive potential of compound **14b** and **14c** against SARS-CoV-2, a comprehensive analysis of the different interactions formed between the active site and the potent compound was conducted during a 100 ns simulation time. Within the simulation trajectory, ligand–residue interactions greater than 30% are referred as protein–ligand contacts. The compound **14b** formed prominent hydrophobic interactions with LYS277 (40%) of 6VWW receptor (Fig. 11). Moreover, **14c** displayed moderate hydrophobic bonding interactions with TRP886 and TYR904 of spike protein (Fig. S52, ESI†). Additionally, **14c** formed strong hydrophobic as well as hydrogen bonding interactions with LYS97 (53%) and PHE150 (66%) (Fig. 12).

The stable protein–ligand complexes are formed as a result of these significant interactions duration the MD simulation.

3 Materials and methods

3.1. Materials

The analytical-grade solvents, chemicals, and reagents (purity ≥ 99%) used throughout this investigation were sourced from Sigma-Aldrich. The NMR signals are denoted as singlet (s), doublet (d), triplet (t) and multiplet (m). The value of J (coupling constant) is given in hertz (Hz). For thin layer chromatography, aluminum plates precoated with silica gel 60F-254 (Merck) were employed, and the resulting chromatograms were visualized under UV illumination at 254 nm to 365 nm. Melting point determinations were performed using a Gallenkamp apparatus. An AVANCE AV 400 MHz spectrometer was used to record NMRs of all synthesized compounds. MS spectra were tracked in Agilent 6400 series (triple quadrupole) instrument. CE-440 Elemental analyzer was used to determine (CHN) elemental analysis.

3.2. Synthesis of substituted 4-methyl-2-oxo-2*H*-chromen-7-yl-2-((4-phenyl-4*H*-1,2,4-triazol-3-yl)thio) acetate 14(a–h)

A mixture of 4-methyl-2-oxo-2*H*-chromen-7-yl-2-bromoacetate (**8**, 0.22 mmol) in DCM was combined with various 4-phenyl-4*H*-1,2,4-triazole-3-thiols (**13a–h**, 0.21 mmol) and K_2CO_3 (0.23 mmol). The reaction mixture was agitated at room temperature for 20 hours. The reaction progression was tracked using thin-layer chromatography (TLC). Upon reaching completion, the target compounds (**14a–h**) were isolated by adding distilled
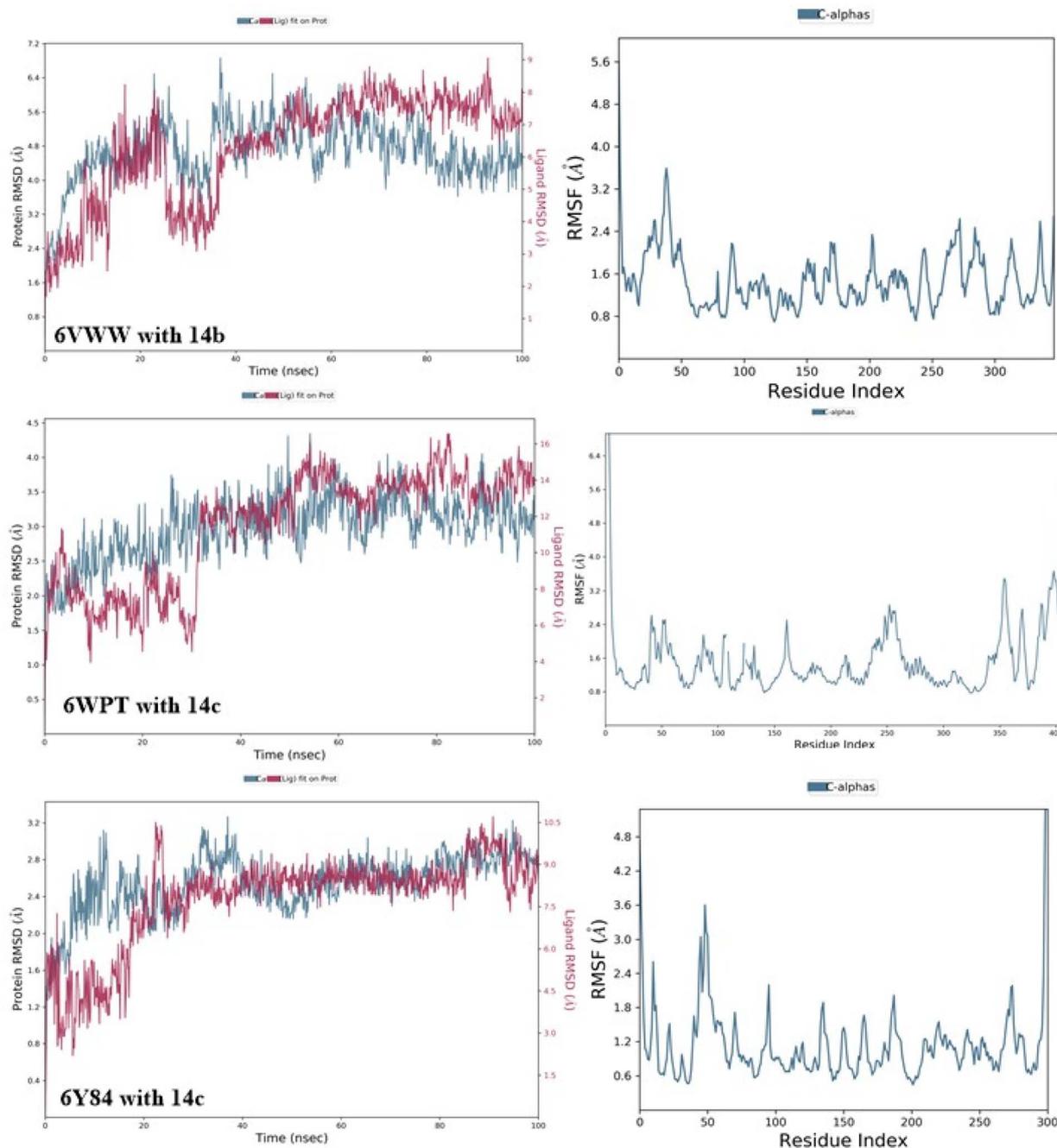
Fig. 10 RMSD and RMSF plots of **14b** and **14c** with 6VWW, 6WPT and 6Y84.

water and *n*-hexane to the reaction mixture, inducing precipitation. The resulting solids were collected through filtration, dried, and subsequently recrystallized from ethanol.

3.3. Synthesis of substituted 2-((4-methyl-2-oxo-2*H*-chromen-7-yl)oxy)-*N*-(*p*-tolyl)acetamide 17(a–h)

The reaction was performed by dissolving 7-hydroxy-4-methylcoumarin (**7**, 0.0045 mol) and various 2-bromo-*N*-phenylacetamides (**16a–h**, 0.0045 mol) in DMF (6 mL) in the presence of K_2CO_3 (0.0049 mol) as a base. The reaction mixture was

stirred at ambient temperature for 22 hours, with periodic assessment of reaction progress *via* TLC. After the reaction was complete, the target compounds (**17a–h**) were isolated as precipitates by adding water to the reaction mixture. The precipitates were washed with water, dried, and then crystallized from ethanol to access the pure compounds.

3.4. *In silico* studies

The synthesized coumarin scaffolds underwent computational molecular docking analysis to assess their binding affinity and
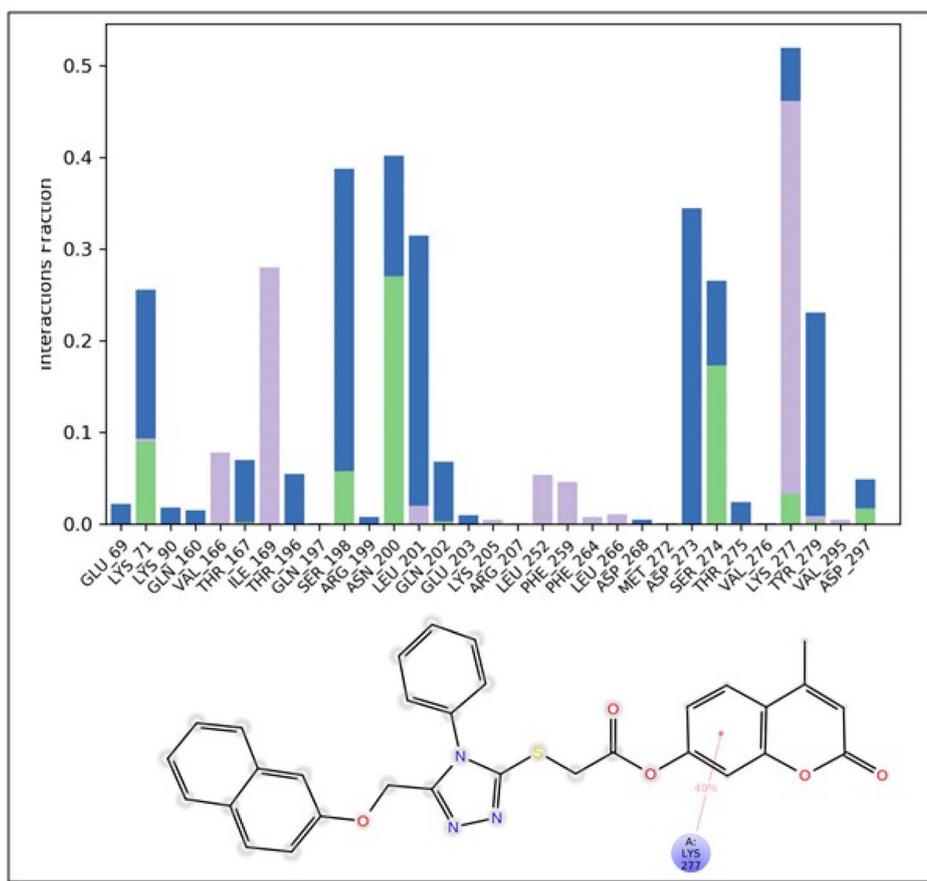
Fig. 11 Protein–ligand contacts plot of **14b** with 6VWW receptor.

anti-SARS-CoV-2 potential. Docking studies were performed with Autodock Vina 1.1.2.[89] The 3D crystallized protein structures (6Y84, 6VWW, and 6WPT) were downloaded from PDB (Protein Data Bank). The standards (chloroquine lopinavir, remdesivir, favipiravir, nirmatrelvir) and targeted compound structures were drawn *via* ChemDraw software. The AutoDock Tools package was utilized to find the binding pocket by using grid box. The search grids for 6Y84, 6VWW, and 6WPT were determined as follows: 6Y84 ($x = 11.869$, $y = 0.552$, $z = 4.89$), 6VWW ($x = -71.795$, $y = 21.929$, $z = -24.02$), and 6WPT ($x = 211.008$, $y = 222.549$, $z = -172.693$), all with 40 xyz dimensions. The exhaustiveness was set to 8 for all targeted receptors.[90–92] The poses with the lowest binding scores were chosen for further ligand–protein interaction study using Discovery Studio v24.1.0.23298. MD (molecular dynamics) simulations (100 ns) were run to determine stability of all the protein–ligand complexes. All the complexes were prepared using Maestro (academic version) from Schrödinger LLC, which corrected structural irregularities. MD simulations were performed by using Desmond module in order to examine the conformational changes and dynamic properties of complexes. The Desmond[93] system builder module was utilized to launch orthorhombic cubic box and solvent model (TIP3P).[94] Counterions (Na+ and Cl−) were incorporated to attain charge neutrality, and 0.15 M

NaCl was added to simulate isotonic conditions.[95] The system underwent energy minimization using the OPLS2005 force field,[96] followed by a 100 ns molecular dynamics simulation at 1 atm pressure and 300 K temperature, generating 1000 trajectories, which were then analyzed using the Simulation Interaction Diagram (SID) tool to compute RMSD, RMSF, and protein–ligand contacts.

4 Conclusion

To conclude, two series of coumarin derivatives **14(a–h)** & **17(a–h)** have been synthesized in good to excellent yields ranging from 51–75% for **14(a–h)** and 62–82% for **17(a–h)**. All of these hybrids **14(a–h)** & **17(a–h)** were docked against three targets known as 6WPT (spike protein), 6Y84 (main-protease) and 6VWW (Nsp15). Remarkable potency was exhibited by **14b** and **14c** against the selected targets, even better than all chosen standards (chloroquine, lopinavir, remdesivir, favipiravir, and nirmatrelvir). Compounds **14b** and **14c** interacted with their respective targets, 6VWW and 6Y84/6WPT, by forming hydrogen bonds and hydrophobic interactions. Molecular dynamic simulations were performed to assess the conformational stability and binding efficacy of potent inhibitors, as determined by RMSD, RMSF and ligand–protein contact analysis.
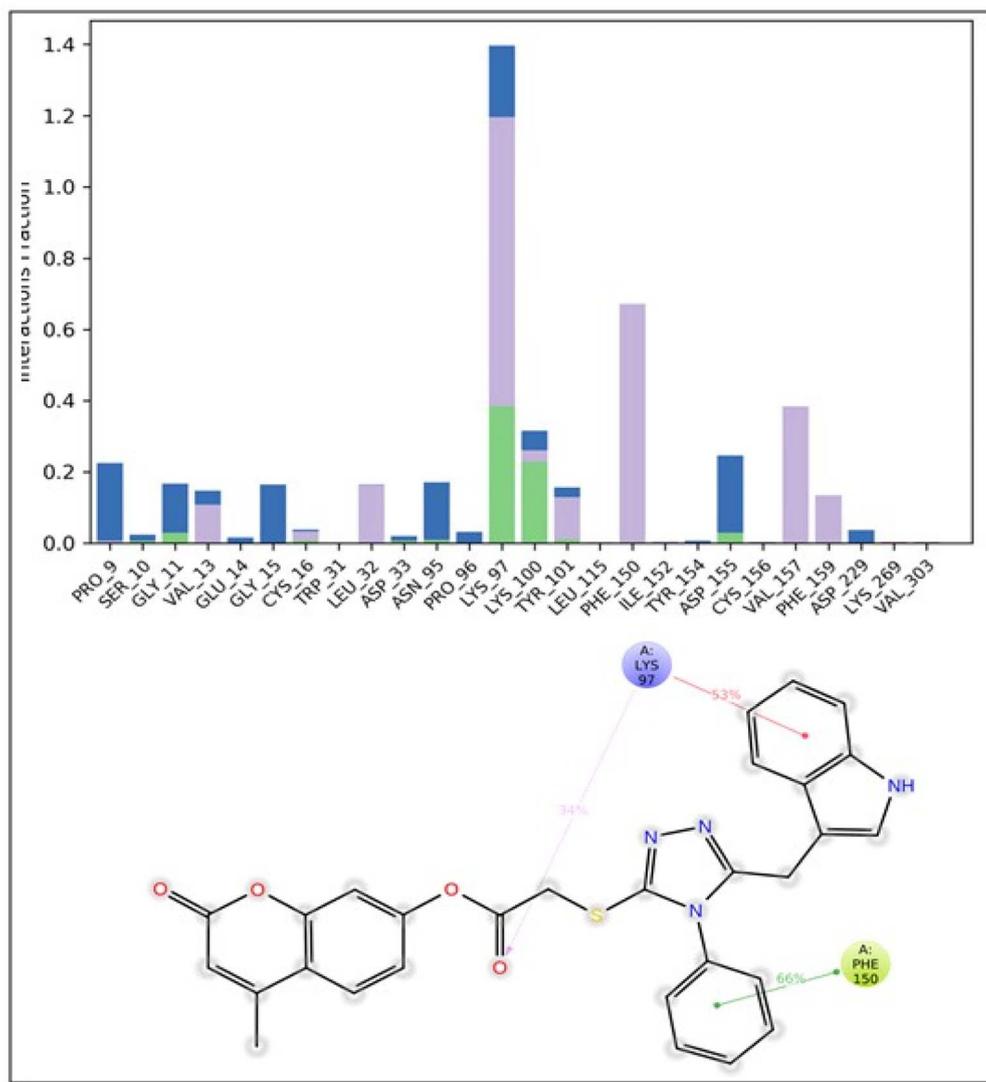
Fig. 12 Protein–ligand contacts plot of **14c** with 6Y84 receptor.

The results of this computational study predict that the compounds **14b** and **14c** merit further investigations through *in vitro* and *in vivo* assays to evaluate their potential as therapeutic agents against SARS-CoV-2.

Data availability

All data is contained in the manuscript and ESI.†

Conflicts of interest

Authors have no conflict of interest for this research work.

References

1 World Health Organization, *WHO Coronavirus Disease (COVID-19) Dashboard*, **https://covid19.who.int/**.
2 O. Delardas, K. Kechagias, P. Pontikos and P. Giannos, *Sustainability*, 2022, **14**, 9699.
3 F. He, Y. Deng and W. Li, *J. Med. Virol.*, 2020, **92**, 719–725.
4 M. M. Khan, M. R. Amin, A. Al Mamun and A. A. Sajib, *J. Software Eng. Appl.*, 2021, **14**, 26.
5 J. Liu and S. Liu, *J. Med. Virol.*, 2020, **92**, 1484–1490.
6 W.-j. Guan, Z.-y. Ni, Y. Hu, W.-h. Liang, C.-q. Ou, J.-x. He, L. Liu, H. Shan, C.-l. Lei and D. S. Hui, *N. Engl. J. Med.*, 2020, **382**, 1708–1720.
7 S. Chavez, B. Long, A. Koyfman and S. Y. Liang, *Am. J. Emerg. Med.*, 2021, **44**, 220–229.
8 H. Ouassou, L. Kharchoufa, M. Bouhrim, N. E. Daoudi, H. Imtara, N. Bencheikh, A. ELbouzidi and M. Bnouham, *J. Immunol. Res.*, 2020, **2020**, 1357983.
9 V. A. Verma, *J. Mol. Struct.*, 2024, **1309**, 138268.
10 N. Zhu, D. Zhang, W. Wang, X. Li, B. Yang, J. Song, X. Zhao, B. Huang, W. Shi and R. Lu, *N. Engl. J. Med.*, 2020, **382**, 727–733.
11 D. Wu, T. Wu, Q. Liu and Z. Yang, *Int. J. Infect. Dis.*, 2020, **94**, 44–48.

12 F. Li, *Annu. Rev. Virol.*, 2016, **3**, 237–261.

13 R. J. Hulswit, C. A. de Haan and B.-J. Bosch, *Adv. Virus Res.*, 2016, **96**, 29–57.

14 R. N. Kirchdoerfer, C. A. Cottrell, N. Wang, J. Pallesen, H. M. Yassine, H. L. Turner, K. S. Corbett, B. S. Graham, J. S. McLellan and A. B. Ward, *Nature*, 2016, **531**, 118–121.

15 I. Glowacka, S. Bertram, P. Herzog, S. Pfefferle, I. Steffen, M. O. Muench, G. Simmons, H. Hofmann, T. Kuri and F. Weber, *J. Virol.*, 2010, **84**, 1198–1205.

16 Z. Liu, H. Zheng, H. Lin, M. Li, R. Yuan, J. Peng, Q. Xiong, J. Sun, B. Li, J. Wu, L. Yi, X. Peng, H. Zhang, W. Zhang, R. J. G. Hulswit, N. Loman, A. Rambaut, C. Ke, T. A. Bowden, O. G. Pybus and J. Lu, *J. Virol.*, 2020, **94**, e00790.

17 S. Matsuyama and F. Taguchi, *J. Virol.*, 2002, **76**, 11819–11826.

18 I. Glowacka, S. Bertram, M. A. Müller, P. Allen, E. Soilleux, S. Pfefferle, I. Steffen, T. S. Tsegaye, Y. He and K. Gnirss, *J. Virol.*, 2011, **85**, 4122–4134.

19 E. Lontok, E. Corse and C. E. Machamer, *J. Virol.*, 2004, **78**, 5913–5922.

20 X. Tian, C. Li, A. Huang, S. Xia, S. Lu, Z. Shi, L. Lu, S. Jiang, Z. Yang and Y. Wu, *Emerging Microbes Infect.*, 2020, **9**, 382–385.

21 B. Cosar, Z. Y. Karagulleoglu, S. Unal, A. T. Ince, D. B. Uncuoglu, G. Tuncer, B. R. Kilinc, Y. E. Ozkan, H. C. Ozkoc and I. N. Demir, *Cytokine Growth Factor Rev.*, 2022, **63**, 10–22.

22 W. T. Harvey, A. M. Carabelli, B. Jackson, R. K. Gupta, E. C. Thomson, E. M. Harrison, C. Ludden, R. Reeve, A. Rambaut and C.-G. U. Consortium, *Nat. Rev. Microbiol.*, 2021, **19**, 409–424.

23 L. Van Dorp, M. Acman, D. Richard, L. P. Shaw, C. E. Ford, L. Ormond, C. J. Owen, J. Pang, C. C. Tan and F. A. Boshier, *Infect., Genet. Evol.*, 2020, **83**, 104351.

24 S. Thakur, S. Sasi, S. G. Pillai, A. Nag, D. Shukla, R. Singhal, S. Phalke and G. Velu, *Front. Biomed.*, 2022, **9**, 815389.

25 Y. Kaku, M. S. Yo, J. E. Tolentino, K. Uriu, K. Okumura, J. Ito and K. Sato, *Lancet Infect. Dis.*, 2024, **24**, e482–e483.

26 Y. Cao, F. Jian, J. Wang, Y. Yu, W. Song, A. Yisimayi, J. Wang, R. An, X. Chen and N. Zhang, *Nature*, 2023, **614**, 521–529.

27 A. Sethi, S. Sanam, S. Munagalasetty, S. Jayanthi and M. Alvala, *RSC Adv.*, 2020, **10**, 29873–29884.

28 V. Mody, J. Ho, S. Wills, A. Mawri, L. Lawson, M. C. Ebert, G. M. Fortin, S. Rayalam and S. Taval, *Commun. Biol.*, 2021, **4**, 93.

29 J. Köppke, L.-E. Keller, M. Stuck, N. D. Arnow, N. Bannert, J. Doellinger and O. Cingöz, *Nat. Commun.*, 2024, **15**, 299.

30 P. Colson, J.-M. Rolain, J.-C. Lagier, P. Brouqui and D. Raoult, *Int. J. Antimicrob. Agents*, 2020, **55**, 105932.

31 C. A. Devaux, J.-M. Rolain, P. Colson and D. Raoult, *Int. J. Antimicrob. Agents*, 2020, **55**, 105938.

32 M. Huang, T. Tang, P. Pang, M. Li, R. Ma, J. Lu, J. Shu, Y. You, B. Chen and J. Liang, *J. Mol. Cell Biol.*, 2020, **12**, 322–325.

33 S. Meini, A. Pagotto, B. Longo, I. Vendramin, D. Pecori and C. Tascini, *J. Clin. Med.*, 2020, **9**, 2050.

34 B. Cao, Y. Wang, D. Wen, W. Liu, J. Wang, G. Fan, L. Ruan, B. Song, Y. Cai and M. Wei, *N. Engl. J. Med.*, 2020, **382**, 1787–1799.

35 S. Saghir and Z. Xiao, *Bioresour. Technol.*, 2024, **391**, 129916.

36 J. H. Beigel, K. M. Tomashek, L. E. Dodd, A. K. Mehta, B. S. Zingman, A. C. Kalil, E. Hohmann, H. Y. Chu, A. Luetkemeyer and S. Kline, *N. Engl. J. Med.*, 2020, **383**, 1813–1826.

37 J. J. Malin, I. Suárez, V. Priesner, G. Fätkenheuer and J. Rybniker, *Clin. Microbiol. Rev.*, 2020, **34**, e00162.

38 A. Rezagholizadeh, S. Khiali, P. Sarbakhsh and T. Entezari-Maleki, *Eur. J. Pharmacol.*, 2021, **897**, 173926.

39 S. Joshi, J. Parkar, A. Ansari, A. Vora, D. Talwar, M. Tiwaskar, S. Patil and H. Barkate, *Int. J. Infect. Dis.*, 2021, **102**, 501–508.

40 B. Dadonaite, J. Brown, T. E. McMahon, A. G. Farrell, M. D. Figgins, D. Asarnow, C. Stewart, J. Lee, J. Logue and T. Bedford, *Nature*, 2024, **631**, 617–626.

41 S. Hassanipour, M. Arab-Zozani, B. Amani, F. Heidarzad, M. Fathalipour and R. Martinez-de-Hoyo, *Sci. Rep.*, 2021, **11**, 11022.

42 R. Arbel, Y. Wolff Sagy, M. Hoshen, E. Battat, G. Lavie, R. Sergienko, M. Friger, J. G. Waxman, N. Dagan and R. Balicer, *N. Engl. J. Med.*, 2022, **387**, 790–798.

43 J. Hammond, H. Leister-Tebbe, A. Gardner, P. Abreu, W. Bao, W. Wisemandle, M. Baniecki, V. M. Hendrick, B. Damle and A. Simón-Campos, *N. Engl. J. Med.*, 2022, **386**, 1397–1408.

44 C. Marzolini, D. R. Kuritzkes, F. Marra, A. Boyle, S. Gibbons, C. Flexner, A. Pozniak, M. Boffito, L. Waters and D. Burger, *Clin. Pharmacol. Ther.*, 2022, **112**, 1191–1200.

45 W. L. Jorgensen, *Science*, 2004, **303**, 1813–1818.

46 M. P. Gleeson, *J. Med. Chem.*, 2008, **51**, 817–834.

47 J. D. Durrant and J. A. McCammon, *BMC Biol.*, 2011, **9**, 1–9.

48 J. Vamathevan, D. Clark, P. Czodrowski, I. Dunham, E. Ferran, G. Lee, B. Li, A. Madabhushi, P. Shah and M. Spitzer, *Nat. Rev. Drug Discovery*, 2019, **18**, 463–477.

49 Z. Sajid, M. Ahmad, S. Aslam, U. A. Ashfaq, A. F. Zahoor, F. A. Saddique, M. Parvez, A. Hameed, S. Sultan and H. Zgou, *Pharm. Chem. J.*, 2016, **50**, 172–180.

50 S. Faiz and A. F. Zahoor, *Mol. Diversity*, 2016, **20**, 969–987.

51 S. Ahmad, A. F. Zahoor, S. A. R. Naqvi and M. Akash, *Mol. Diversity*, 2018, **22**, 191–205.

52 I. Rasool, M. Ahmad, Z. A. Khan, A. Mansha, T. Maqbool, A. F. Zahoor and S. Aslam, *Trop. J. Pharm. Res.*, 2017, **16**, 723–733.

53 A. Kanwal, F. A. Saddique, S. Aslam, M. Ahmad, A. F. Zahoor and N.-u.-A. Mohsin, *Pharm. Chem. J.*, 2018, **51**, 1068–1077.

54 P. S. Mishra, A. Kumar, K. Kaur and V. Jaitak, *Curr. Med. Chem.*, 2024, **31**, 5702–5738.

55 H. Ma, K. Wang, B. Wang, Z. Wang, Y. Liu and Q. Wang, *J. Agric. Food Chem.*, 2024, **72**, 4658–4668.

56 N. N. Kamel, H. F. Aly, G. I. Fouad, S. S. Abd El-Karim, M. M. Anwar, Y. M. Syam, S. A. Elseginy, K. A. Ahmed, H. F. Booles and M. B. Shalaby, *RSC Adv.*, 2023, **13**, 18496–18510.

57 P. P. Song, J. Zhao, Z. L. Liu, Y. B. Duan, Y. P. Hou, C. Q. Zhao, M. Wu, M. Wei, N. H. Wang and Y. Lv, *Pest Manage. Sci.*, 2017, **73**, 94–101.

58 A. Sahar, Z. A. Khan, M. Ahmad, A. F. Zahoor, A. Mansha and A. Iqbal, *Trop. J. Pharm. Res.*, 2017, **16**, 203–210.

59 R. Kausar, A. F. Zahoor, H. Tabassum, S. Kamal and M. Ahmad Bhat, *Pharmaceuticals*, 2024, **17**, 532.

60 S. Saeed, M. J. Saif, A. F. Zahoor, H. Tabassum, S. Kamal, S. Faisal, R. Ashraf, S. G. Khan, U. Nazeer and A. Irfan, *RSC Adv.*, 2024, **14**, 15419–15430.

61 R. Z. Batran, A. Sabt, J. Dziadek and A. F. Kassem, *RSC Adv.*, 2024, **14**, 21763–21777.

62 A. Irfan, S. Faiz, A. Rasul, R. Zafar, A. F. Zahoor, K. Kotwica-Mojzych and M. Mojzych, *Molecules*, 2022, **27**, 1023.

63 A. Wu, K. Shi, J. Wang, R. Zhang and Y. Wang, *Eur. J. Med. Chem.*, 2024, **263**, 115923.

64 K. Sharma, M. Singh, P. Sharma, S. C. Sharma, S. Mujwar, M. Kapoor, K. K. Mishra and T. A. Wani, *Molecules*, 2024, **29**, 1406.

65 S. Chidambaram, M. A. El-Sheikh, A. H. Alfarhan, S. Radhakrishnan and I. Akbar, *Saudi J. Biol. Sci.*, 2021, **28**, 1100–1108.

66 M. S. Bekheit, S. S. Panda, B. M. Kariuki, S. H. Mahmoud, A. Mostafa and A. S. Girgis, *Eur. J. Med. Chem.*, 2023, **258**, 115563.

67 K. B. Lokhande, S. Doiphode, R. Vyas and K. V. Swamy, *J. Biomol. Struct. Dyn.*, 2021, **39**, 7294–7305.

68 K. Shinohara, T. Kobayakawa, K. Tsuji, Y. Takamatsu, H. Mitsuya and H. Tamamura, *Eur. J. Med. Chem.*, 2024, **280**, 116963.

69 S. Saeedi, A. Rahmati and Z. Chavoshpour-Natanzi, *RSC Adv.*, 2022, **12**, 19579–19589.

70 S. De Vita, M. G. Chini, G. Lauro and G. Bifulco, *RSC Adv.*, 2020, **10**, 40867–40875.

71 S. Koulgi, V. Jani, M. V. Uppuladinne, U. Sonavane and R. Joshi, *RSC Adv.*, 2020, **10**, 26792–26803.

72 L. C. Assis, A. A. de Castro, J. P. A. de Jesus, E. F. F. da Cunha, E. Nepovimova, O. Krejcar, K. Kuca, T. C. Ramalho and F. d. A. La Porta, *RSC Adv.*, 2021, **11**, 35228–35244.

73 H. S. Elbordiny, N. Z. Alzoman, H. M. Maher and S. I. Aboras, *RSC Adv.*, 2023, **13**, 26719–26731.

74 O. M. Ogunyemi, G. A. Gyebi, I. M. Ibrahim, C. O. Olaiya, J. O. Ocheje, M. M. Fabusiwa and J. O. Adebayo, *RSC Adv.*, 2021, **11**, 33380–33398.

75 S. Sonadevi, D. Rajaraman, M. Saritha, P. Solo and L. Athishu Anthony, *Mol. Phys.*, 2025, **123**, e2353331.

76 D. Douche, Y. Sert, S. A. Brandán, A. A. Kawther, B. Bilmez, N. Dege, A. El Louzi, K. Bougrin, K. Karrouchi and B. Himmi, *J. Mol. Struct.*, 2021, **1232**, 130005.

77 A. Rani, G. Singh, A. Singh, U. Maqbool, G. Kaur and J. Singh, *RSC Adv.*, 2020, **10**, 5610–5635.

78 M. M. Abdelshaheed, H. I. El Subbagh, M. A. Tantawy, R. T. Attia, K. M. Youssef and I. M. Fawzy, *RSC Adv.*, 2023, **13**, 15689–15703.

79 F. Shiri, S. Shahraki, S. Baneshi, M. Nejati-Yazdinejad and M. H. Majd, *RSC Adv.*, 2016, **6**, 106516–106526.

80 S. Jalil, Z. Hussain, S. M. A. Abid, A. Hameed and J. Iqbal, *RSC Adv.*, 2024, **14**, 8905–8920.

81 M. Maddah, R. Bahramsoltani, N. H. Yekta, R. Rahimi, R. Aliabadi and M. Pourfath, *New J. Chem.*, 2021, **45**, 15977–15995.

82 S. Kumar, P. Kashyap, S. Chowdhury, S. Kumar, A. Panwar and A. Kumar, *Phytomedicine*, 2021, **85**, 153317.

83 M. Saeed, A. Saeed, M. J. Alam and M. Alreshidi, *Molecules*, 2020, **25**, 5657.

84 B. Gopi and V. Vijayakumar, *RSC Adv.*, 2024, **14**, 13218–13226.

85 D. P. Tran, Y. Taira, T. Ogawa, R. Misu, Y. Miyazawa and A. Kitao, *Sci. Rep.*, 2022, **12**, 3860.

86 S. Skariyachan, D. Gopal, S. Chakrabarti, P. Kempanna, A. Uttarkar, A. G. Muddebihalkar and V. Niranjan, *Comput. Biol. Med.*, 2020, **126**, 104054.

87 S. Skariyachan, D. Gopal, A. G. Muddebihalkar, A. Uttarkar and V. Niranjan, *Comput. Biol. Med.*, 2021, **132**, 104325.

88 B. N. Marak, J. Dowarah, L. Khiangte and V. P. Singh, *Drug Dev. Res.*, 2021, **82**, 374–392.

89 T. Gaillard, *J. Chem. Inf. Model.*, 2018, **58**, 1697–1706.

90 G. Wang, Z. Peng, J. Wang, X. Li and J. Li, *Eur. J. Med. Chem.*, 2017, **125**, 423–429.

91 T. N. H. Pham, T. H. Nguyen, N. M. Tam, T. Y. Vu, N. T. Pham, N. T. Huy, B. K. Mai, N. T. Tung, M. Q. Pham and V. V. Vu, *J. Comput. Chem.*, 2022, **43**, 160–169.

92 J. Ding, S. Tang, Z. Mei, L. Wang, Q. Huang, H. Hu, M. Ling and J. Wu, *J. Chem. Inf. Model.*, 2023, **63**, 1982–1998.

93 Y. Ali, A. A. Khan, A. M. Alanazi, S. A. Abdikakharovich, J. A. Shah, Z.-G. Ren and S. Khattak, *Mol. Diversity*, 2024, 1–14.

94 Y. Moukhliss, Y. Koubi, M. Alaqarbeh, N. Alsakhen, S. Hamzeh, H. Maghat, A. Sbai, M. Bouachrine and T. Lakhlifi, *New J. Chem.*, 2022, **46**, 10154–10161.

95 B. Jójárt, R. Kiss, B. Viskolcz, I. Kolossváry and G. r. M. Keserű, *J. Phys. Chem. Lett.*, 2010, **1**, 1008–1013.

96 Y. Hua, X. Tan, J. Zhang, N. Xu, R. Chen, S. Zhou, S. Liu, K. Li, W. Chen and Q. Luo, *Sci. Rep.*, 2024, **14**, 29873.